

Quantum phase transitions, Excitonic supersolid and its detections in electron-hole bilayer systems

Jinwu Ye

Department of Physics, The Pennsylvania State University, University Park, PA, 16802

(Dated: February 9, 2022)

We construct a quantum Ginsburg-Landau theory to study the quantum phases and transitions in electron hole bilayer system. We propose that in the dilute limit as distance is increased, there is a first order transition from the excitonic superfluid (ESF) to the excitonic supersolid (ESS) driven by the collapsing of a roton minimum, then a 2nd order transition from the ESS to excitonic normal solid. We show the latter transition is in the same universality class of superfluid to Mott transition in a rigid lattice. We then study novel elementary low energy excitations inside the ESS. We find that there are two "supersolidon" longitudinal modes (one upper branch and one lower branch) inside the ESS, while the transverse mode in the ESS stays the same as that inside a ENS. We also work out various experimental signatures of these novel elementary excitations by evaluating the Debye-Waller factor, density-density correlation, specific heat and vortex-vortex interactions. For the meta-stable supersolid generated by photon pumping, we show that the angle resolved spectrum is dominated by the macroscopic super-radiance from its superfluid component, even it is just a very small percentage of the whole system. This fact can be used to detect the metastable ESS state generated by photon pumping by a power spectrum experiment easily and without any ambiguity.

I. INTRODUCTION

Recently, degenerate exciton systems have been produced by different experimental groups with different methods in quasi-two-dimensional semiconductor *GaAs/AlGaAs* coupled quantum wells structure^{1,2,3,4,5}. There are two different ways to generate the excitons. One is through photon pumping, then applying an electric field along z direction to confine electrons in one quantum well and holes in another quantum well^{1,2,3}. We call these kind of excitons as photon generated excitons. The second is through gate voltage^{4,5}. We call these kind of excitons as gate voltage generated excitons. When the distance between the two quantum wells is sufficiently small, an electron in one well and a hole in the other well could pair to form an exciton which behaves as a boson at long distance. Now it was widely believed that the electron-hole bilayer (EHBL) is a very promising system to observe Bose-Einstein condensation (BEC) of excitons. For simplicity, we only discuss balanced el-hole bilayers where the electrons and holes have the same density $n_e = n_h$, but may have different masses $m_e \neq m_h$. The case with different masses and with different density is also very interesting and will be investigated in separate publications.

There are two important dimensionless parameters in the EHBL. One is the dimensionless distance $\gamma = d/a_B$ (a_B is the Bohr radius) between the two layers. Another is r_s which is the ratio of the kinetic energy over the potential energy in a single layer. The $r_s a_B$ is the typical interparticle distance in a single layer. It is easy to see that the ratio of intralayer Coulomb V_{11} over the interlayer Coulomb V_{12} interactions $\alpha = V_{11}/V_{12} = d/r_s a_B$. So when the interlayer Coulomb interaction dominates $\alpha < 1$, the EHBL is expected to exhibit the superfluid of excitons. If the density of excitons is sufficiently low (large r_s), then the system is in a weakly coupled Wigner

solid state at very large distance and become an BEC excitonic superfluid (ESF) at short distance (Fig.1). An interesting problem is how the system evolves from the BEC ESF to the weakly coupled Wigner solid as the distance increases. If an exciton is already formed, its kinetic energy $K \sim \frac{\hbar^2}{m^*(r_s a_B)^2}$, its potential energy $P \sim \frac{e^2 d^2}{\epsilon(r_s a_B)^3}$. When $K < P$, namely, $\sqrt{r_s} < d/a_B$, the EHBL could favor a excitonic (or dipolar) normal solid (ENS) state. As argued above, when $d/a_B < r_s$, the EHBL is in a ESF state. So in the intermediate distance $\sqrt{r_s} < d/a_B < r_s$ ⁹, the system may favor a excitonic (or dipolar) supersolid (ESS) state. When $d/a_B > r_s$, it will become the excitonic normal solid (ENS) due to the long range dipole-dipole $1/r^3$ repulsive interactions (Fig.1). A hole system with $r_s \sim 20 - 30$ was already realized⁶. If $r_s \sim 20 \gg 1$ limit, there is a broad distance regime $4.5 < d/a_B < 20$, the system could be in the ESS state. It becomes feasible to experimentally explore all the possible phases and phase transitions in the EHBL in the near future.

It was originally pointed out in¹³ that for any supersolid to exist, there must be quantum fluctuations generated vacancies even in the ground state of a solid at $T = 0$. Obviously, the first candidate to search for supersolid is near the phase boundary of superfluid ⁴He and solid ⁴He. The authors in¹⁴ suggested that the supersolid state leads to the non-classical rotational inertia (NCRI) observed in the torsional oscillator experiment, many other experiments such as neutron scattering, X-ray diffraction, mass flow, heat capacity, acoustic sound attenuation and so on are needed to uniquely distinguish the supersolid from other enormous number of much less interesting possibilities. A phenomenological quantum Ginzburg-Landau theory¹⁵ was developed to make predictions on signatures of these experiments if the supersolid indeed exists in Helium 4. Unfortunately, so far,

all these experiments came as negative. It becomes interesting to see if a supersolid state can exist in other systems which also have both superfluid state and solid state. In this paper, we will point out that the excitons in EHBL may be a very promising experimental system to observe the excitonic supersolid (ESS) near the phase boundary between the ESF and the ENS. Because the exciton's mass $m_{ex} = 0.37m_e$ is much smaller than that of ${}^4\text{He}$, so the zero point quantum fluctuations in the ENS in EHBL is even much larger than those in solid Helium 4. I will point out a new mechanism which is absent in ${}^4\text{He}$ to generate repulsive excitonic vacancies in the ENS which leads to the intermediate excitonic supersolid (ESS) phase in the dilute limit in the EHBL. Then we construct a quantum Ginzburg-Landau theory to study all the phases and quantum phase transitions in Fig.1. It is instructive to compare the EHBL system with the pseudo-spin sector in the bilayer quantum Hall system (BLQH) at total filling factor $\nu_T = 1$. Although the ESF in Fig.1 shares some common properties with the corresponding ESF in the BLQH^{10,11,12}, due to different symmetries of the two systems, translational symmetry breaking states are very different. For example, ESS and ENS phases which are the focus of this paper have no analogies in the BLQH. These crucial differences will be explicitly studied in the following. Furthermore, in sharp contrast to BLQH which is a stable system, for the photon generated excitons, the excitonic phases in Fig.1 are just meta-stable states which will eventually decay by emitting lights. We will show that the angle resolved power spectrum from the internal photon can detect the ESS unanimously if it indeed exists. In fact, the characteristics of emitted photons is a very natural, feasible and unambiguous internal probe of all the three phases ESF, ESS and the ENS in Fig.1.

The paper is organized as follows. In sec. II, we derive the quantum Ginzburg-Landau action to describe the transition from the ESF to the ENS driven by the collapsing of a roton minimum. Then In Sec.III, we will argue that in general there should be a ESS state intervening between the ESF and the ENS. In Sec.IV, by renormalization group analysis, we study the universality class of zero temperature quantum phase transition from ENS to ESS driven by the distance. In Sec.V, we work out the elementary low energy excitations inside the supersolids. Then in the following sections, we study the experimental signatures of these low energy excitations by calculating the Debye-Waller factor in the X-ray scattering from the ESS in sec. VI, the density-density correlation function in the ESS in sec.VII. In Sec.VIII, we study the specific heat in the ESS. In Sec. IX, by performing a duality transformation to the vortex representation, we will study the vortices in the ESS. In Sec.X, we will present the photon emission pattern from the ESS formed by photon pumping generated excitons. Finally, we reach conclusions in Sec.XI.

II. THE ZERO TEMPERATURE TRANSITION FROM ESF TO ENS DRIVEN BY THE DISTANCE

If $c_1(c_2)$ is the electron annihilation operator in top (bottom) layer, then $h_2^\dagger = c_2$ is the hole creation operator in the bottom layer. The order parameter for the ESF is the $p-h$ pairing $\psi(\vec{x}, \tau) = \langle c_1^\dagger c_2 \rangle = \langle c_1^\dagger h_2^\dagger \rangle = \sqrt{\bar{\rho} + \delta\rho} e^{i\theta(\vec{x}, \tau)}$. The effective action inside the ESF is essentially the same as that in the pseudo-spin channel in BLQH¹⁰:

$$\mathcal{L}[\delta\rho, \theta] = i\delta\rho\partial_\tau\theta + \frac{1}{2}\rho_d(\nabla\theta)^2 + \frac{1}{2}\delta\rho V_d(\vec{q})\delta\rho \quad (1)$$

In the ESF state, it is convenient to integrate out $\delta\rho$ in favor of the phase field θ to get the phase representation:

$$\mathcal{L}[\theta] = \frac{1}{2V_d(\vec{q})}(\partial_\tau\theta)^2 + \rho_d(\nabla\theta)^2 \quad (2)$$

where the dispersion relation of the Goldstone modes including higher orders of momentum can be extracted:

$$\omega^2 = [2\rho_d V_d(\vec{q})]q^2 \quad (3)$$

In the long wavelength limit, $V_d(\vec{q} \rightarrow 0) \rightarrow c$ (c is a constant) (Fig.1) leads to a capacitive term for the density fluctuation. The QMC calculations^{7,8} indeed find that there is a roton minimum in the dispersion relation (Fig.1).

Because the original instability comes from the density-density interaction $V_d(\vec{q})$, it is convenient to integrate out the phase field in favor of the density operator in the original action Eqn.1. Neglecting the vortex excitations in θ and integrating out the θ in Eqn.1 leads to:

$$\mathcal{L}[\delta\rho] = \frac{1}{2}\delta\rho(-\vec{q}, -\omega_n) \left[\frac{\omega_n^2}{2\rho_d q^2} + V_d(\vec{q}) \right] \delta\rho(\vec{q}, \omega_n) \quad (4)$$

where we can identify the dynamic density-density correlation function:

$$S(\vec{q}, \omega_n) = \langle \delta\rho(-\vec{q}, -\omega_n) \delta\rho(\vec{q}, \omega_n) \rangle = \frac{2\rho_d q^2}{\omega_n^2 + v^2(q)q^2} \quad (5)$$

where $v^2(q) = 2\rho_d V_d(q)$ is the spin wave velocity defined in Eqn.3.

From the pole of the dynamic density-density correlation function, we can identify the speed of sound wave which is exactly the same as the spin wave velocity. This should not be too surprising. As shown in liquid ${}^4\text{He}$, the speed of sound is exactly the same as the phonon velocity. Here, in the context of excitonic superfluid, we explicitly prove that the sound speed is indeed the same as the spin wave velocity.

From the analytical continuation $i\omega_n \rightarrow \omega + i\delta$ in Eqn.5, we can identify the dynamic structure factor: $S(\vec{q}, \omega) = S(q)\delta(\omega - v(q)q)$ where $S(q) = \rho_d q\pi/v(q)$ is the equal time density correlation function shown in Fig.1.

As $q \rightarrow 0, S(q) \rightarrow q$. The Feymann relation in the ESF which relates the dispersion relation to the equal time structure factor is

$$\omega(q) = \frac{\rho_d \pi q^2}{S(q)} \quad (6)$$

which takes exactly the same form as the Feymann relation in superfluid 4He . Obviously, the $V_d(q)$ in the Fig.1b leads to the roton dispersion $\omega^2 = q^2 V_d(q)$ in the Fig.1a.

Because the instability happens near $q = q_0$ instead of $q = 0$, so the transition in Fig.1 is *not* driven by vortex unbinding transitions like in 3D XY model, so the vortices remain tightly bound near the transition. So integrating out the vortex excitations in θ will only generate *weak* interactions among the density $\delta\rho$:

$$\begin{aligned} \mathcal{L}[\delta\rho] = & \frac{1}{2} \delta\rho(-\vec{q}, -\omega) \left[\frac{\omega_n^2}{2\rho_d q^2} + V_d(\vec{q}) \right] \delta\rho(\vec{q}, \omega) \\ & - w(\delta\rho)^3 + u(\delta\rho)^4 + \dots \end{aligned} \quad (7)$$

where the momentum and frequency conservation in the quartic and sixth order term is assumed.

Expanding $V_d(q)$ near the roton minimum q_0 leads to the quantum Ginsburg-Landau action to describe the ESF to the ENS transition:

$$\mathcal{L}[\delta\rho] = \frac{1}{2} \delta\rho [A_\rho \omega^2 + r + c(q^2 - q_0^2)^2] \delta\rho - w(\delta\rho)^3 + u(\delta\rho)^4 + \dots \quad (8)$$

where $A_\rho \sim \frac{1}{2\rho_d q_0^2}$ which is non-critical across the transition. In sharp contrast to the ESF to the pseudo-spin density wave (PSDW) transition in BLQH¹⁰, because of the lack of Z_2 exchange symmetry between the two layers in EHBL, there is a cubic term in Eqn.8. It was explicitly shown in¹⁸ that in the presence of both the cubic and the quartic terms, the favorable lattice is a triangular lattice instead of a square lattice in PSDW¹⁰. The generic transition driven by the collapsing of roton minimum is from ESF to ENS instead of from the ESF to the excitonic supersolid (ESS). In the ESF, $\langle r \rangle = 0, \langle \psi \rangle \neq 0, \langle \delta\rho \rangle = 0$. In the ENS, $r < 0, \langle \psi \rangle = 0, \langle \delta\rho \rangle = \sum'_{\vec{G}} n_{\vec{G}} e^{i\vec{G}\cdot\vec{x}}$ where \vec{G} is the 6 shortest reciprocal lattice vector of a triangular lattice (Fig.1).

III. EXISTENCE OF ESS INTERVENING BETWEEN THE ESF AND ENS.

In the section, I point out a mechanism to generate excitonic vacancies which lead to a narrow window of ESS intervening between the ESF and the ENS. As the distance increases to the critical distance d_{c1} , because the lattice constant $r_s a_B$ is completely fixed by the parameter r_s which is *independent of* the distance which drives the transition, so the resulting state is likely to have vacancies with density $n_v(0)$ even at $T = 0$. By contrast, in solid Helium 4, the density is self-determined

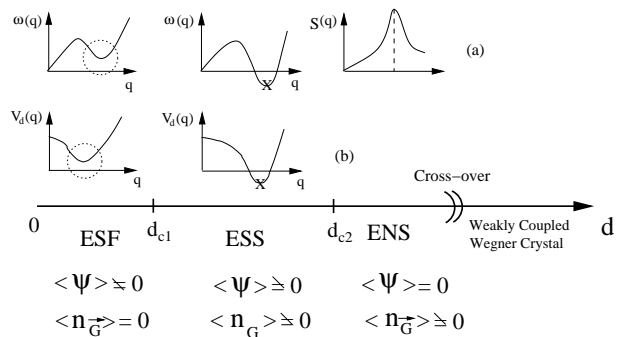


FIG. 1: The zero temperature phase diagram in the SEHB as the distance between the two layers increases. ESF where $\langle \psi \rangle \neq 0, \langle n_{\vec{G}} \rangle = 0$ stands for excitonic superfluid, ESS where $\langle \psi \rangle \neq 0, \langle n_{\vec{G}} \rangle \neq 0$ stands for excitonic supersolid phase, ENS where $\langle \psi \rangle = 0, \langle n_{\vec{G}} \rangle \neq 0$ stands for exciton normal solid phase. (a) Energy dispersion relation $\omega(q)$ in these phases. (b) the bare dipole-dipole interaction $V_d(q)$ in these phases. The cross in the ESS means the negative minimum value of $V_d(q)$ is replaced by the ESS state. The order parameters are also shown. Also shown in far right in (a) is the equal time structure factor $S(q)$. In fact, the instability happens before the minimum touches zero. The generic transition driven by the collapsing of roton minimum is the ESF to ENS transition. However, as argued in the text, there could be a window of ESS intervening between the ESF and the ENS.

by the pressure $n = \frac{\partial P}{\partial \mu}|_{T,V}$, so the density and pressure go hand in hand, the solid 4He is likely to be commensurate. We expect that the vacancy-vacancy interaction is also a repulsive dipole-dipole one. It is the condensation of these repulsively interacting vacancies at $T = 0$ which leads to the SF mode $\psi(\vec{x}, \tau)$ inside the *incommensurate* ENS. This resulting state is the ESS state where $\langle \psi \rangle \neq 0, \langle \delta\rho \rangle \neq 0$ (Fig.1). As the distance increases to $d_{c2} > d_{c1}, n_v(0) = 0$, the resulting state is a *commensurate* ENS whose lattice constant is still *locked* at $r_s a_B$ (Fig.1). As distance increases further, the ENS will crossover to the two weakly coupled Wigner crystal. Note that because $V_d(\vec{q} \rightarrow 0) \rightarrow c$, the phonon spectrum is still $\omega \sim q$ instead of $\sim q^{3/2}$ as claimed in⁹. Very similar argument was used in¹⁰ to conclude that there should be zero-point quantum fluctuations generated vacancies in the pseudo-spin density wave (PSDW) in BLQH. By contrast, due to the absence of the cubic term, the lattice is a square lattice. In the PSDW, the vacancies are essentially fermionic holes, so can not condensate. It is the correlated hopping of vacancies in the active and passive layers in the PSDW state which leads to very large and temperature dependent drag consistent with the experimental data.

The finite temperature phase diagram corresponding to Fig.1 is shown in Fig.2. At any finite T , the ESF will only have algebraic long range order and will turn into a normal liquid (NL) by a Kosterlitz-Thouless (KT) transition. ENS may go through a hexatic phase before melting into a NL phase. The finite temperature phases

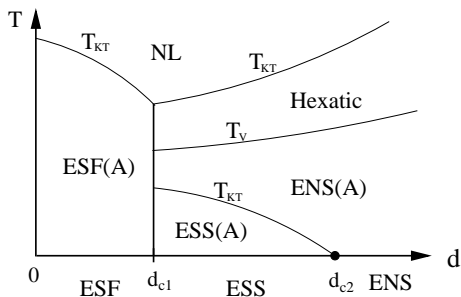


FIG. 2: The finite temperature phase diagram in the SEHB as the distance between the two layers increases. ESF(A) means only algebraic off-diagonal long range order (ODLRO), ESS(A) means only algebraic ODLRO and algebraic translational order. ENS(A) means only algebraic translational order. Hexatic phase has the algebraic orientational order, but no translational order. NL is the normal liquid phase. T_{KT} is the KT transition. T_V is the vector Coulomb gas transition. The dot is the zero temperature transition from the ENS to the ESS investigated in section 4.

and phase transitions above the ESS phase in the intermediate distance $d_{c1} < d < d_{c2}$ is also shown in Fig.2.

IV. THE ZERO TEMPERATURE TRANSITION FROM ESS TO ENS DRIVEN BY THE DISTANCE.

The effective action to describe the ENS to ESS transition at $T = 0$ consistent with all the lattice symmetries and the global $U(1)$ symmetry is:

$$\begin{aligned} \mathcal{L} = & \psi^\dagger \partial_\tau \psi + c_{\alpha\beta} \partial_\alpha \psi^\dagger \partial_\beta \psi + r |\psi|^2 + g |\psi|^4 \\ & + \frac{1}{2} \rho_n (\partial_\tau u_\alpha)^2 + \frac{1}{2} \lambda_{\alpha\beta\gamma\delta} u_{\alpha\beta} u_{\gamma\delta} \\ & + a_{\alpha\beta}^0 u_{\alpha\beta} \psi^\dagger \partial_\tau \psi + a_{\alpha\beta}^1 u_{\alpha\beta} |\psi|^2 + \dots \end{aligned} \quad (9)$$

where $r = d - d_{c2}$ (Fig. 1), ρ_n is the normal density, $u_{\alpha\beta} = \frac{1}{2}(\partial_\alpha u_\beta + \partial_\beta u_\alpha)$ is the linearized strain tensor, $\lambda_{\alpha\beta\gamma\delta}$ are the bare elastic constants dictated by the symmetry of the lattice, it has 2 independent elastic constants for a triangular lattice where $\lambda_{\alpha\beta\gamma\delta} = \lambda \delta_{\alpha\beta} \delta_{\gamma\delta} + \mu (\delta_{\alpha\gamma} \delta_{\beta\delta} + \delta_{\alpha\delta} \delta_{\beta\gamma})$ where λ and μ are Lamé coefficients. In the ENS state $r > 0$, $\langle \psi(\vec{x}, \tau) \rangle = 0$, the 2 lattice phonon modes $\vec{u}(\vec{x}, \tau)$ become the 2 ordinary ones. While inside the ESS state $r < 0$, $\langle \psi(\vec{x}, \tau) \rangle \neq 0$. If setting all the couplings between ψ and u_α vanish, the ψ sector describes the SF to Mott insulator transition in a *rigid* underlying two dimensional lattice studied in¹⁷. Under the Renormalization group (RG) transformation, $\tau' = \tau/b^z$, $x' = x/b$ and $\psi' = \psi/Z$. If we choose $z = 2$, $Z = b^{-d/2}$, the $g' = gb^{2-d}$. We also choose $u'_\alpha = u_\alpha/Z$, then $\rho'_n = b^{-2}\rho_n$, so the lattice phonon kinetic energy term is irrelevant near the QCP. It is easy to see $a'_0 = b^{-d/2-1}a_0$, so a_0 is always irrelevant. $a'_1 = b^{1-d/2}a_1$, so both g and a_1 's upper critical dimension is $d_u = 2$, so we can perform a $\epsilon = 2 - d$ expansion

in both g and a_1 . The RG equations are found to be:

$$\frac{dg}{dl} = \epsilon g - cg^2; \quad \frac{da_1}{dl} = \frac{\epsilon}{2} a_1 \quad (10)$$

where $c = 2mK_d \Lambda^{d-2}/\hbar^2$ is the same constant as that in the rigid model¹⁷. So a_1 is exactly marginal without affecting the universality class. This is can also be understood as follows: because ρ_n is irrelevant, so we can simply integrate out u_α which only leads to a shift of the value of g . We conclude that the ENS to ESS transition stays in the same universality class of the superfluid to Mott insulator transition at $d = 2$ in a rigid lattice which has the mean field exponents $z = 2, \nu = 1/2, \eta = 0$ with logarithmic corrections. For example, the superfluid density inside the ESS should scale as $\rho_s \sim |d_{c2} - d|^{(d+z-2)\nu} = |d_{c2} - d|$ with a logarithmic correction.

If neglecting the τ dependence by setting $u_\alpha(\vec{x}, \tau) = u_\alpha(\vec{x})$, $\psi_0(\vec{x}, \tau) = \psi_0(\vec{x})$, then Eqn.9 reduces to the classical action. For the classical case, $x' = x/b$, $\psi' = \psi/Z$, $u'_\alpha = u_\alpha/Z$, if we choose $Z = b^{(2-d)/2}$, then $g' = gb^{4-d}$, $a'_1 = b^{2-d/2}a_1$, so both g and a_1 's upper critical dimension is $d_u = 4$. So in principle, a $\epsilon = 4 - d$ expansion is possible for both g and a_1 , the putting $\epsilon = 2$ for $d = 2$. It is known that due to the essential singularity of the KT transition, the specific heat exponent of the KT transition $\alpha = -\infty < 0$, the $a_{\alpha\beta}^1$ coupling is irrelevant, so the ENS to ESS transition remains to be Kosterlitz-Thouless (KT) transition at finite temperature. This conclusion is consistent with the RG analysis at $T = 0$ in the last paragraph. The quantum critical scalings near the ENS to the ESS transition at $d = d_{c2}$ can be worked out along the similar lines in²⁰.

V. THE LOW ENERGY EXCITATIONS IN THE ESS

In this section, we will study the low energy elementary excitations in the ESS. Inside the ESS, $\langle \psi_0(\vec{x}, \tau) \rangle = a$, we can write $\psi_0(\vec{x}, \tau) = \sqrt{a + \delta\rho} e^{i\theta(\vec{x}, \tau)}$ and plug it into the Eqn.9. Integrating out the massive magnitude $\delta\rho$ fluctuations and simplifying, we get the effective action describing the low energy modes inside the SS phase:

$$\begin{aligned} \mathcal{L} = & \frac{1}{2} [\rho_n (\partial_\tau u_\alpha)^2 + \lambda_{\alpha\beta\gamma\delta} u_{\alpha\beta} u_{\gamma\delta}] \\ & + \frac{1}{2} [\kappa (\partial_\tau \theta)^2 + \rho_{\alpha\beta}^s \partial_\alpha \theta \partial_\beta \theta] + a_{\alpha\beta} u_{\alpha\beta} i \partial_\tau \theta \end{aligned} \quad (11)$$

where κ is the SF compressibility and $\rho_{\alpha\beta}^s$ is the SF stiffness which has the same symmetry as $a_{\alpha\beta}^0$, $a_{\alpha\beta} = a_{\alpha\beta}^0 + S_0 a_{\alpha\beta}^1$ where $S_0(\vec{k}, \omega)$ is the bare SF density correlation function. Obviously, the last term is the crucial coupling term which couples the lattice phonon modes to the SF mode. The factor of i is important in this coupling. By integration by parts, this term can also be written as $a_{\alpha\beta} (\partial_\tau u_\beta \partial_\alpha \theta + \partial_\tau u_\alpha \partial_\beta \theta)$ which has the clear

physical meaning of the coupling between the SF velocity $\partial_\alpha \theta$ and the velocity of the lattice vibration $\partial_\tau u_\beta$. It is this term which makes the low energy modes in the SS to have its own characteristics which could be detected by experiments. In this section, we neglect the topological vortex line excitations in Eqn.11. In section IX, we will discuss these vortex line excitations in detail. In the following, we discuss triangular lattice specifically.

For a triangular lattice, $\lambda_{\alpha\beta\gamma\delta} = \lambda\delta_{\alpha\beta}\delta_{\gamma\delta} + \mu(\delta_{\alpha\gamma}\delta_{\beta\delta} + \delta_{\alpha\delta}\delta_{\beta\gamma})$ where λ and μ are Lamé coefficients, $\rho_{\alpha,\beta}^s = \rho^s\delta_{\alpha,\beta}$, $a_{\alpha,\beta} = a\delta_{\alpha,\beta}$. In (\vec{q}, ω_n) space, the Eqn.11 becomes:

$$\begin{aligned} \mathcal{L}_{is} = & \frac{1}{2}[\rho_n\omega_n^2 + (\lambda + 2\mu)q^2]|u_l(\vec{q}, \omega_n)|^2 \\ & + \frac{1}{2}[\kappa\omega_n^2 + \rho_s q^2]|\theta(\vec{q}, \omega_n)|^2 \\ & + 2a q \omega_n u_l(-\vec{q}, -\omega_n)\theta(\vec{q}, \omega_n) \\ & + \frac{1}{2}[\rho_n\omega_n^2 + \mu q^2]|u_t(\vec{q}, \omega_n)|^2 \end{aligned} \quad (12)$$

where $u_l(\vec{q}, \omega_n) = iq_i u_i(\vec{q}, \omega_n)/q$, $u_t(\vec{q}, \omega_n) =$

$i\epsilon_{ij}q_i u_j(\vec{q}, \omega_n)/q$ are the longitudinal and transverse components of the displacement field respectively. Note that Eqn.12 shows that only the longitudinal component couples to the superfluid θ mode, while the transverse component is unaffected by the superfluid mode. This is expected, because the superfluid mode is a longitudinal density mode itself which does not couple to the transverse modes.

From Eqn.12, we can identify the longitudinal-phonon correlation function:

$$\langle u_l u_l \rangle = \frac{\kappa\omega_n^2 + \rho_s q^2}{(\kappa\omega_n^2 + \rho_s q^2)(\rho_n\omega_n^2 + (\lambda + 2\mu)q^2) + a^2 q^2 \omega_n^2} \quad (13)$$

The $\langle \theta\theta \rangle$ and $\langle u_l\theta \rangle$ correlation functions can be similarly written down. By doing the analytical continuation $i\omega_n \rightarrow \omega + i\delta$, we can identify the two poles of all the correlation functions at $\omega_\pm^2 = v_\pm^2 q^2$ where the two velocities v_\pm is given by:

$$v_\pm^2 = [\kappa(\lambda + 2\mu) + \rho_s \rho_n + a^2 \pm \sqrt{(\kappa(\lambda + 2\mu) + \rho_s \rho_n + a^2)^2 - 4\kappa\rho_s\rho_n(\lambda + 2\mu)}] / 2\kappa\rho_n \quad (14)$$

If setting $a = 0$, then c_\pm^2 reduces to the longitudinal phonon velocity $v_{lp}^2 = (\lambda + 2\mu)/\rho_n$ and the superfluid velocity $v_s^2 = \rho_s/\kappa$ respectively. Of course, the transverse phonon velocity $v_{tp}^2 = \mu/\rho_n$ is untouched. For notation simplicity, in the following, we just use v_p for v_{lp} . Inside the ESS, due to the very small superfluid density ρ_s , it is expected that $v_p > v_s$. It is easy to show that $v_+ > v_p > v_s > v_-$ and $v_+^2 + v_-^2 > v_p^2 + v_s^2$, but $v_+ v_- = v_p v_s$, so $v_+ + v_- > v_p + v_s$ (see Fig.3).

In principle, inelastic neutron scattering experiments or acoustic attenuation experiments can be used to detect the predicted the low energy excitation spectra in the SS shown in Fig.3.

VI. DEBYE-WALLER FACTOR IN THE X-RAY SCATTERING FROM THE ESS

It is known that due to zero-point quantum motion in any NS at very low temperature, the X-ray scattering amplitude $I(\vec{G})$ will be diminished by a Debye-Waller (DW) factor $\sim e^{-\frac{1}{2}G^2\langle u_\alpha^2 \rangle}$ at $d = 2$ where u_α is the lattice phonon modes in Eqn.11. In Eqn.11, if the coupling between the \vec{u} and θ were absent, then the DW factor in the SS would be the same as that in the NS. By taking the ratio $I_{SS}(\vec{G})/I_{NS}(\vec{G})$ at a given reciprocal lattice vector \vec{G} , then this DW factor drops out. Due to the presence of this coupling, the $\langle u_\alpha^2 \rangle$ in SS is different than

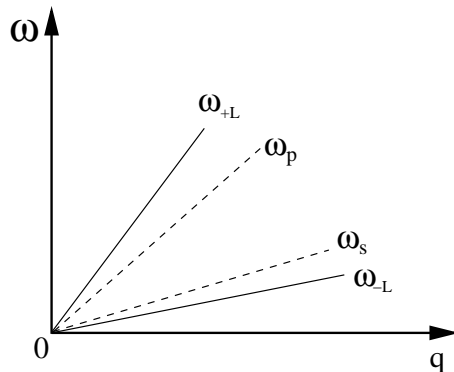


FIG. 3: The elementary low energy excitation inside a excitonic supersolid (ESS). The coupling between the phonon mode $\omega_p = v_p q$ (the upper dashed line) and the superfluid mode $\omega_s = v_s q$ (the lower dashed line) leads to the two new longitudinal modes $\omega_\pm = v_\pm q$ (solid lines) in the ESS. The transverse mode stays the same as that in the ENS and is not shown.

that in NS, so the DW factor will *not* drop out in the ratio. In this section, we will calculate this ratio and see how to take care of this factor when comparing with the X-ray scattering data.

The density order parameter at the reciprocal lattice vector \vec{G} is $\rho_{\vec{G}}(\vec{x}, \tau) = e^{i\vec{G}\cdot\vec{u}(\vec{x}, \tau)}$, then $\langle \rho_{\vec{G}}(\vec{x}, \tau) \rangle =$

$e^{-\frac{1}{2}G_i G_j \langle u_i u_j \rangle}$. The Debye-Waller factor:

$$I(\vec{G}) = |\langle \rho_{\vec{G}}(\vec{x}, \tau) \rangle|^2 = e^{-G_i G_j \langle u_i(\vec{x}, \tau) u_j(\vec{x}, \tau) \rangle} \quad (15)$$

where the phonon-phonon correlation function is:

$$\langle u_i u_j \rangle = \langle u_i u_l \rangle \hat{q}_i \hat{q}_j + \langle u_t u_t \rangle (\delta_{ij} - \hat{q}_i \hat{q}_j) \quad (16)$$

where $\hat{q}_i \hat{q}_j = \frac{q_i q_j}{q^2}$.

Then substituting Eqn.16 into Eqn.15 leads to:

$$\alpha(\vec{G}) = I_{SS}(\vec{G})/I_{NS}(\vec{G}) = e^{-\frac{1}{2}G^2[\langle u_l^2(\vec{x}, \tau) \rangle_{SS} - \langle u_l^2(\vec{x}, \tau) \rangle_{NS}]} \quad (17)$$

where the transverse mode drops out, because it stays the same in the SS and in the NS.

Defining $(\Delta u^2)_l(\vec{q}, i\omega_n) = \langle |u_l(\vec{q}, i\omega_n)|^2 \rangle_{SS} - \langle |u_l(\vec{q}, i\omega_n)|^2 \rangle_{NS}$, $(\Delta u^2)_l(\vec{q}) = \sum_{i\omega_n} (\Delta u^2)_l(\vec{q}, i\omega_n)$ and $(\Delta u^2)_l = \langle u_l^2(\vec{x}, \tau) \rangle_{SS} - \langle u_l^2(\vec{x}, \tau) \rangle_{NS} = \int \frac{d^2 q}{(2\pi)^2} \frac{1}{\beta} \sum_{i\omega_n} (\Delta u^2)_l(\vec{q}, i\omega_n) = \int \frac{d^2 q}{(2\pi)^2} (\Delta u^2)_l(\vec{q})$, it is easy to see:

$$(\Delta u^2)_l = \int \frac{d^2 q}{(2\pi)^2} \frac{1}{\beta} \sum_{i\omega_n} \frac{-a^2 q^2 \omega_n^2}{[(\kappa \omega_n^2 + \rho_s q^2)(\rho_n \omega_n^2 + (\lambda + 2\mu)q^2) + a^2 q^2 \omega_n^2][\rho_n \omega_n^2 + (\lambda + 2\mu)q^2]} \quad (18)$$

Obviously, $(\Delta u^2)_l < 0$, namely, the longitudinal vibration amplitude in SS is *smaller* than that in NS. Then $\alpha(\vec{G})(T=0) = e^{-\frac{1}{2}G^2(\Delta u^2)_l} > 1$. This is expected, because the SS state is the ground state at $T < T_{SS}$, so the longitudinal vibration amplitude should be reduced compared to the corresponding NS with the same parameters ρ_n, λ, μ .

After evaluating the frequency summation in Eqn.18, we get:

$$(\Delta u^2)_l(T) = \int \frac{d^2 q}{(2\pi)^2} \frac{1}{\rho_n} \left[\frac{\coth \beta v_+ q/2}{2v_+ q} - \frac{\coth \beta v_p q/2}{2v_p q} - \left(\frac{v_s^2 - v_-^2}{v_+^2 - v_-^2} \right) \left(\frac{\coth \beta v_+ q/2}{2v_+ q} - \frac{\coth \beta v_- q/2}{2v_- q} \right) \right] \quad (19)$$

At $T=0$, the above equation simplifies to:

$$\begin{aligned} (\Delta u^2)_l(T=0) &= \int \frac{d^2 q}{(2\pi)^2} \frac{1}{\rho_n} \left[\frac{1}{2v_+ q} - \frac{1}{2v_p q} - \left(\frac{v_s^2 - v_-^2}{v_+^2 - v_-^2} \right) \left(\frac{1}{2v_+ q} - \frac{1}{2v_- q} \right) \right] \\ &= -\frac{(v_+ + v_- - v_p - v_s)}{(v_+ + v_-)v_p} \frac{\Lambda}{4\pi\rho_n} \\ &= -\frac{a^2}{\kappa\rho_n} \frac{1}{(v_+ + v_- + v_p + v_s)(v_+ + v_-)v_p} \frac{\Lambda}{4\pi\rho_n} < 0 \quad (20) \end{aligned}$$

where $\Lambda \sim 1/a$ is the ultra-violet cutoff and we have used the fact $v_+ + v_- > v_p + v_s$.

At finite T , in Eqn.19, if taking $q \rightarrow 0$ limit, it is easy to see the integrand identically vanishes. So Eqn.19 is well defined.

VII. DENSITY-DENSITY CORRELATIONS

The density-density correlation function in the SS is:

$$\langle \rho_{\vec{G}}(\vec{x}, t) \rho_{\vec{G}}^*(\vec{x}', t') \rangle = e^{-\frac{1}{2}G_i G_j \langle (u_i(\vec{x}, t) - u_i(\vec{x}', t'))(u_j(\vec{x}, t) - u_j(\vec{x}', t')) \rangle} \quad (21)$$

where t is the real time.

For simplicity, we only evaluate the equal-time correlator $\langle \rho_{\vec{G}}(\vec{x}, t) \rho_{\vec{G}}^*(\vec{x}', t) \rangle = \langle \rho_{\vec{G}}(\vec{x}, \tau) \rho_{\vec{G}}^*(\vec{x}', \tau) \rangle$ where τ is the imaginary time. It is instructive to compare the density order in SS with that in a NS by looking at the ratio of the density correlation function in the SS over the NS:

$$\alpha_\rho(\vec{x} - \vec{x}') = \langle \rho_{\vec{G}} \rho_{\vec{G}}^* \rangle_{SS} / \langle \rho_{\vec{G}} \rho_{\vec{G}}^* \rangle_{NS} = e^{-\frac{1}{4}G^2 \Delta D_\rho(\vec{x} - \vec{x}')} \quad (22)$$

It is easy to find that

$$\Delta D_\rho(\vec{x} - \vec{x}') = \int \frac{d^2 q}{(2\pi)^2} (2 - e^{i\vec{q} \cdot (\vec{x} - \vec{x}')} - e^{-i\vec{q} \cdot (\vec{x} - \vec{x}')}) (\Delta u^2)_l(\vec{q}) \quad (23)$$

where $(\Delta u^2)_l(\vec{q})$ is defined above Eqn.18 and is the integrand in Eqn.19.

At $T=0$, the above equation can be simplified to

$$\Delta D_\rho(\vec{x} - \vec{x}') = \frac{(v_+ + v_- - v_p - v_s)}{(v_+ + v_-)v_p} \frac{1}{2\pi\rho_n} \frac{1}{|\vec{x} - \vec{x}'|} \quad (24)$$

So we conclude that $\alpha_\rho(\vec{x} - \vec{x}') < 1$, namely, the density order in SS is *weaker* than the NS with the corresponding parameters ρ_n, λ, μ . This is expected because the density order in the SS is weakened by the presence of moving vacancies.

It is known that there is only algebraic order instead of true solid order at any finite T , so the algebraic decay exponent in ESS stays the same as that in ENS.

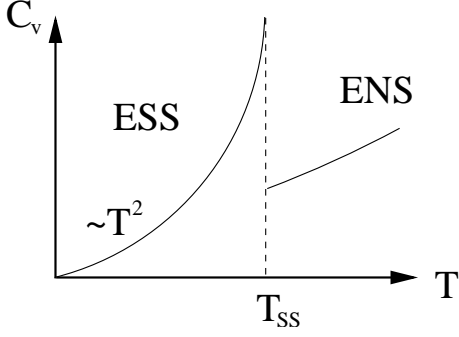


FIG. 4: Specific heat in ENS and ESS. The area below C_v/T from $T = 0$ to $T = T_{SS}$ is the entropy in the ESS. The excess entropy is due to the lower branch

VIII. SPECIFIC HEAT IN THE ESS

It is easy to see that at low T , the specific heat in the ENS

$$C^{NS} = C_{lp}^{NS} + C_{tp}^{NS} + C_{van} \quad (25)$$

where $C_{lp}^{NS} = \frac{3}{\pi}\zeta(3)k_B(\frac{k_B T}{\hbar v_{lp}})^2$ is due to the longitudinal phonon mode where $\zeta(3) = 1.202$ and $C_{tp}^{NS} = \frac{3}{\pi}\zeta(3)k_B(\frac{k_B T}{\hbar v_{tp}})^2$ is due to the transverse phonon mode, while C_{van} is from the vacancy contribution. It is still not known how to calculate C_{van} yet. The specific heat in the SF $C_v^{SF} = \frac{3}{\pi}\zeta(3)k_B(\frac{k_B T}{\hbar v_s})^2$ is due to the SF mode θ . From Eqn.12, we can find the specific heat in the ESS:

$$C_v^{SS} = \frac{3}{\pi}\zeta(3)k_B(\frac{k_B T}{\hbar v_+})^2 + \frac{3}{\pi}\zeta(3)k_B(\frac{k_B T}{\hbar v_-})^2 + C^{tp} \quad (26)$$

where C^{tp} stands for the contributions from the transverse phonons which are the same as those in the ENS.

It was argued in¹⁵, the critical regime of finite temperature NS to SS transition in Fig.1 is much narrower than the that of SF to the NL transition, so there should be a jump in the specific heat at $T = T_{SS}$. Eqn.26 shows that at $T < T_{SS}$, the specific heat still takes $\sim T^2$ behavior and is dominated by the ω_- mode in Fig.2.

From Eqn.26, it is easy to evaluate the entropy inside the ESS:

$$S_{SS}(T_{SS}) = \frac{3}{2\pi}\zeta(3)k_B(\frac{k_B T_{SS}}{\hbar})^2(\frac{1}{v_+^2} + \frac{1}{v_-^2}) + S^{tp} \quad (27)$$

where S^{tp} is the entropy due to the transverse mode.

From Eqn.25 and 26, we find that the *excess* entropy due to the vacancy condensation is:

$$\Delta S = \int_0^{T_{SS}} dT C_{van}/T = \frac{3}{2\pi}\zeta(3)k_B(\frac{k_B T_{SS}}{\hbar})^2(\frac{1}{v_+^2} + \frac{1}{v_-^2} - \frac{1}{v_{lp}^2}) \quad (28)$$

Obviously, $\Delta S > 0$ is due to the lower branch $v_- < v_{lp}$. At $a = 0$, the above equation reduces to $\Delta S = \frac{3}{2\pi}\zeta(3)k_B(\frac{k_B T_{SS}}{\hbar v_s})^2$ which is simply due to the vacancy condensation into ESF.

IX. VORTICES IN THE EXCITONIC SUPERSOLID

In section 5, we studied the low energy excitations shown in the Fig.2 by neglecting the topological vortex line excitations. Here, we will study how the vortex line interaction in ESS differ from that in the ESF. We can perform a duality transformation on Eqn.11 to the vortex representation:

$$\mathcal{L}_v = \frac{1}{2K_\mu}(\epsilon_{\mu\nu\lambda}\partial_\nu a_\lambda - a\partial_\alpha u_\alpha \delta_{\mu\tau})^2 + i2\pi a_\mu j_\mu^v \quad (29)$$

where μ, ν, λ stand for space and time, while α, β stand for the space components only, $K_0 = \kappa, K_\alpha = \rho_s$ and a_μ is the 3 component gauge fields and $j_\mu^v = \frac{1}{2\pi}\epsilon_{\mu\nu\lambda}\partial_\nu\partial_\lambda\theta$ is the vortex line current due to the topological phase winding in θ .

Eqn.29 has the gauge invariance $a_\mu \rightarrow a_\mu + \partial_\mu\chi$ where χ is any field. It is most convenient to choose the Coulomb gauge $\partial_\alpha a_\alpha = 0$ to get rid of the longitudinal component, then the transverse component is $a_t = i\epsilon_{\alpha\beta}q_\alpha a_\beta/q$. It can be shown that $|a_t|^2 = |a_\alpha|^2$. Then Eqn.29 becomes:

$$\begin{aligned} \mathcal{L}_v = & \frac{1}{2}[\rho_n\omega_n^2 + (\lambda + 2\mu + a^2/\kappa)q^2]|u_i(\vec{q}, \omega_n)|^2 \\ & + \frac{1}{2}(q^2/\kappa + \omega_n^2/\rho_s)|a_t|^2 + \frac{q^2}{2\rho_s}|a_0|^2 \\ & - aq^2/\kappa u_i(-\vec{q}, -\omega_n)a_t(\vec{q}, \omega_n) \\ & + i2\pi j_0^v a_0 + i2\pi j_\alpha^v a_\alpha \end{aligned} \quad (30)$$

where the transverse phonon mode u_t was omitted, because it stays the same as in the NS as shown in Eqn.12.

It is easy to see that only a_t has the dynamics, while a_0 is static. This is expected, because although a_μ has 3 non-vanishing components, only the transverse component a_t has the dynamics which leads to the original gapless superfluid mode $\omega^2 = v_s^2 q^2$. Eqn.30 shows that it is the longitudinal phonon mode u_l coupled to the transverse gauge mode a_t . The vortex line density is $j_0^v = \frac{1}{2\pi}\epsilon_{\alpha\beta}\partial_\alpha\partial_\beta\theta$ and the vortex current is $j_\alpha^v = -\frac{1}{2\pi}\epsilon_{\alpha\beta}[\partial_0, \partial_\beta]\theta$. Integrating out the a_0 , we get the vortex density-density interaction:

$$\pi\rho_s \int_0^\beta d\tau \int dx dy j_{0\alpha}^v(\vec{x}, \tau) \log|x - y| j_{0\beta}^v(\vec{y}, \tau) \quad (31)$$

Namely, the vortex density-density interaction in SS stays as $\sim \ln r$ which is the same as that in NS! The vortex energy and the critical temperature T_{SS} in Fig. 2 is solely determined by the superfluid density ρ_s only, independent of any other parameters in the action Eqn.12. The critical behaviors of the vortices close to the 2d XY transition was just the well known KT transition.

Integrating out the a_α , we get the vortex current-current interaction:

$$(2\pi)^2/2j_\alpha^v(-\vec{q}, -\omega_n)D_{\alpha\beta}(\vec{q}, \omega_n)j_\beta^v(\vec{q}, \omega_n) \quad (32)$$

where $D_{\alpha\beta}(\vec{q}, \omega_n) = (\delta_{\alpha\beta} - \frac{q_\alpha q_\beta}{q^2}) D_t(\vec{q}, \omega_n)$ where $D_t(\vec{q}, \omega_n)$ is the a_t propagator. Defining $\Delta D_t(\vec{q}, \omega_n) = D_t^{SS}(\vec{q}, \omega_n) - D_t^{SF}(\vec{q}, \omega_n)$ as the difference between the a_t propagator in the ESS and the ESF, then from Eqn.30, we can get:

$$\Delta D_t = \frac{a^2 \rho_s^2 q^4}{\kappa \rho_n (\omega_n^2 + v_+^2 q^2) (\omega_n^2 + v_-^2 q^2) (\omega_n^2 + v_s^2 q^2)} \quad (33)$$

$$\Delta D_t(\vec{x} - \vec{x}', \tau = 0) = \frac{a^2 \rho_s^2}{4\pi \kappa^2 \rho_n^2} \frac{v_+ + v_- + v_s}{(v_+ + v_-)(v_s + v_+)(v_s + v_-)v_+ v_- v_s} \frac{1}{|\vec{x} - \vec{x}'|} \quad (34)$$

Namely, the vortex current-current interaction in SS is stronger than that in the SF with the same parameters κ, ρ_s !

X. DETECTION OF THE ESS BY ITS PHOTON EMISSION PATTERNS.

In the previous sections, we worked out the fundamental properties of the ESS and various experimental signatures of the ESS. These experiments can be performed easily in the gate voltage generated exciton systems in^{4,5}, but it is very hard to perform for the photon pumping generated excitons systems in^{1,2,3} due to the short life time of these kind of excitons. One important question is how to detect the existence of the metastable ESS in Fig.1 if it indeed exists ? In a recent preprint¹⁶, the authors found that when the angle resolved power spectrum (ARPS) from the ESF in the Fig.1 always takes a *macroscopic* superradiance form which is proportional to N^2 . The concept of super-radiance was first proposed by Dicke in 1954 for N two level atomic atoms confined into a small volume V which is much smaller than the wavelength of the emitted photon¹⁹. The macroscopic super-radiance from the ESF even holds in the thermodynamic limit where $N \rightarrow \infty, V \rightarrow \infty$, but keep N/V at finite. This is due to the macroscopic phase coherence of all the N excitons in the whole volume V , so it a completely different mechanism than that of Dicke in conventional quantum optics. This fact can be used to detect the ESS easily in a ARPS experiment for the following reason: the power spectrum from the ENS in Fig.1 is just a normal radiance, so proportional to N_{NS} , however, that from the ESF in Fig.1 is a macroscopic super-radiance, so proportional to N_{vac}^2 . Because the ENS is a uniform phase consisting of a normal solid component and a superfluid component, the ARPS at any given in-plane momentum \vec{k} from the ESS is:

$$S_{ESS}(\vec{k}) \propto N_{vac}^2 + N_{NS} \quad (35)$$

For simplicity, we just give the expression for the equal time:

which takes a Lorentzian form with the photon energy $\omega_k = v_g \sqrt{\vec{k}^2 + k_z^2}$ centering around the exciton gap $E_g \sim 1.545 eV$ ¹⁶.

For a simple estimate, the superfluid component is only a small $\sim 10^{-2}$ component of the whole system, so $N_{vac}/N_{NS} \sim 10^2$, then $S_{ESS}(\vec{k}) \propto N_{NS}(10^{-4}N_{NS} + 1)$. Although 10^{-4} is a very tiny number, but it times a huge number $N_{NS} \sim 10^{10}$ for a $1cm^2$ sample. This leads to the fantastic fact that even the ESF component is just a very small component of the ESS, it *dominates* the ARPS due to its macroscopic super-radiance. So as distance changes in Fig.1, the ARPS along any direction should distinguish the three phases ESF, ESS and ENS easily and without any ambiguity.

It was shown in¹⁶, due to the symmetry breaking in the ESF, the emitted photon along the normal direction is a coherent state. The photon number is proportional to the condensation fraction N_0 . It was also shown that due to the non-vanishing anomalous Green function in the ESF state in Fig.1a, the emitted photons along all tilted directions are always in a two mode squeezed state between \vec{k} and $-\vec{k}$ even off the resonance. The squeezing ratio is proportional to the number of excitons N in the EHBL. All the results are robust and independent of any microscopic details. The detection of the coherent state along the normal direction and the squeezed state along all the tilted directions requires phase sensitive homodyne experiment which is essentially a phase interference experiment between the emitted light and a local reference oscillator. When increasing the distance as shown in the Fig.1, the coherent photons along the normal direction will be much reduced from the ESF to the ESS by 10^{-2} and completely disappear inside the ENS. The two modes squeezing ratio will also be much reduced from the ESF to ENS by 10^{-2} and completely disappear inside the ENS. However, due to the tiny superfluid component inside the ENS, the phase sensitive homodyne experiment to measure the two mode squeezing state inside the ENS is much harder to perform than the angle resolved power spectrum experiment.

In principle, the emitted photons from the ESS will

form a photonic band structure reflecting the periodic triangular lattice structure of the ESS. However as shown in¹⁶, the maximum in-plane wavevector of the emitted photons around energy $E_g \sim 1.545eV$ is at least 2 order of magnitude smaller than the size of the Brillouin Zone of the ESS, so the effect of the underlying lattices is negligibly small.

XI. CONCLUSIONS.

We studied phases and quantum phase transitions in the dilute limit ($r_s \gg 1$) as distance is increased. When the distance is sufficiently small, the system is in the Excitonic superfluid state. When the distance is sufficiently large, it is in the weakly coupled Wigner crystal state. We argued that there is a Excitonic supersolid state intervening between the two phases at some intermediate distance range $\sqrt{r_s} < d/a_B < r_s$. We derive a quantum Ginsburg-Landau action to describe the ESF to the ESS transition driven by the collapsing of the roton minimum. In general, there should be zero-point quantum fluctuations generated vacancies whose condensation lead to the formation of superfluid mode inside the ESS. We then derive the quantum GL action to describe the transition from the ENS at the large distance to the ESS at the intermediate distance. By RG analysis, we showed that the coupling to the quantum fluctuations of the underlying lattice is marginal, so the ENS to the ESS transition is in the same universality class as superfluid to Mott insulator transition in a rigid lattice, therefore has exact exponents $z = 2, \nu = 1/2, \eta = 0$ with logarithmic corrections. We showed that the ESS is a triangular lattice. We then study the elementary excitations inside the ESS. We found that the coupling to quantum lattice phonons is very important inside the ESS and leads to two longitudinal supersolidon modes $\omega_{\pm} = v_{\pm}q$ shown in Fig.3. The transverse modes in the ESS stays the same as those in the ENS. Detecting the two longitudinal modes, especially, the lower branch ω_- mode by neutron scattering or acoustic wave attention experiments is a smoking gun

experiment to prove or disprove the existence of the ESS in the intermediate distance regime. Then we calculated the experimental signature of the two modes. We found that the longitudinal vibration in the ESS is smaller than that in the ENS (with the same corresponding solid parameters), so the Debye-Waller factor at a given reciprocal lattice vector is larger than that in the ENS. The density-density correlation function in the ESS is weaker than that in the ENS. The specific heat in the SS is still given by the sum from the transverse phonons and the two longitudinal phonons and still shows $\sim T^2$ behaviors. The contribution from longitudinal part is dominated by the lower supersolidon branch in Fig.3. By going the to the dual vortex representation, we found the vortex density-density interaction in ESS stays the same as that in the ESF (with the same corresponding superfluid parameters), so the vortex energy and the corresponding ESS(A) to ENS(A) transition temperature T_{KT} in Fig.2 is solely determined by the superfluid density and independent of any other parameters. The vortex current-current interaction in stronger than that in the SF. In principle, all these predictions can be tested by experimental techniques such as X-ray scattering, neutron scattering, acoustic wave attenuations and heat capacity.

For the excitons generated by photon pumping, the ESS is a meta-stable non-equilibrium state, it will decay eventually by emitting photons. The angle resolved power spectrum (ARPS) $S_{ESS}(\vec{k})$ at any given in-plane momentum \vec{k} is dominated by the macroscopic super-radiance from its superfluid component, even the superfluid component is just a very small percentage of the the whole system. In the ESF, ESS and ENS phases in the Fig.1, the ARPS shows the following sequence: $S_{ESF} \sim N^2 \gg S_{ESS} \sim N_{vac}^2 \gg S_{ENS} \sim N$. This sequence can be measured by a ARPS along any direction easily and without any ambiguity.

The research at KITP-C is supported by the Project of Knowledge Innovation Program (PKIP) of Chinese Academy of Sciences.

¹ L. V. Butov *et al*, Nature 417, 47 - 52 (02 May 2002); Nature 418, 751 - 754 (15 Aug 2002); C. W. Lai *et al*, Science 23 January 2004 303: 503-506.
² D. Snoke *et al*, Nature 418, 754 - 757 (15 Aug 2002); David Snoke, Nature 443, 403 - 404 (28 Sep 2006).
³ R. Rapaport *et.al*, Phys. Rev. Lett. 92, 117405 (2004); Gang Chen *et al*, arXiv:cond-mat/0601719.
⁴ U. Sivan, P. M. Solomon, and H. Shtrikman, Phys. Rev. Lett. 68, 1196 - 1199 (1992)
⁵ J. A. Seamons, D. R. Tibbetts, J. L. Reno, M. P. Lilly, , arXiv:cond-mat/0611220.
⁶ Jongsoo Yoon *et al*, Phys. Rev. Lett. 82, 1744C1747 (1999).
⁷ S. De Palo, F. Rapisarda and Gaetano Senatore, Phys. Rev. Lett. 88, 206401 (2002).

⁸ S. De Palo, S. Conti and S. Moroni, Phys. Rev. B 69, 035109 (2004).
⁹ Y. N. Joglekar, A. V. Balatsky, S. Das Sarma, cond-mat/0606124.
¹⁰ Jinwu Ye and Longhua Jiang, Phys. Rev. Lett. 98, 236802 (2007).
¹¹ Jinwu Ye, Phys. Rev. Lett. 97, 236803 (2006).
¹² Jinwu Ye, Annals of Physics, 323 (2008), 580-630.
¹³ G. V. Chester, Phys. Rev. A 2, 256 (1970).
¹⁴ E. Kim and M. H. W. Chan, Science 305, 1941-1944.
¹⁵ Jinwu Ye, cond-mat/0603269.
¹⁶ Si Tao, Jinwu Ye and C. P. Sun, arXiv:0802.1065.
¹⁷ Fisher M. P. A., Weichman P. B., Grinstein G. and Fisher D. S. Phys. Rev. B 40, 546 (1989).

- ¹⁸ Longhua Jiang and Jinwu Ye, Phys. Rev. B 76, 184104 (2007).
- ¹⁹ R. H. Dicke, Phys. Rev. 93, 99 (1954).
- ²⁰ A. Chubukov, S. Sachdev and J. Ye, Phys.Rev.B, 11919 (1994).